Microbubbles Reveal Chiral Fluid Flows in Bacterial Swarms

BIOLOGICAL SCIENCES: Microbiology, Biophysics
PHYSICAL SCIENCES: Applied Physical Sciences

Microbubbles reveal chiral fluid flows in bacterial swarms

Yilin Wu, Basarab G. Hosu, and Howard C. Berg*

Rowland Institute at Harvard, Cambridge, MA 02142 and Department of Molecular and Cellular Biology, Harvard University, Cambridge, MA 02138

*Corresponding author. Mailing address: Department of Molecular and Cellular Biology, Harvard University, 16 Divinity Ave., Cambridge, MA 02138. Phone: (617) 495-0924. Fax: (617) 496-1114. E-mail: hberg@mcb.harvard.edu

Abstract

Flagellated bacteria can swim within a thin film of fluid that coats a solid surface, such as agar; this is a means for colony expansion known as swarming. We found that micron-sized bubbles make excellent tracers for the motion of this fluid. The microbubbles form explosively when small aliquots of an aqueous suspension of droplets of a water-insoluble surfactant (Span 83) are placed on the agar ahead of a swarm, as the water is absorbed by the agar and the droplets are exposed to air. Using these bubbles, we discovered an extensive stream (or river) of swarm fluid flowing clockwise along the leading edge of an *Escherichia coli* swarm, at rates of order 10 μm/s, about three times faster than the swarm expansion. The flow is generated by the action of counterclockwise rotating flagella of cells stuck to the substratum, which drives fluid clockwise around isolated cells (when viewed from above), counterclockwise between cells in dilute arrays, and clockwise in front of cells at the swarm edge. The river provides an avenue for long-range communication in the swarming colony, ideally suited for secretory vesicles that diffuse poorly. These findings broaden our understanding of swarming dynamics and have implications for the engineering of bacterial-driven microfluidic devices.

Key words: microscopic bubbles, bacterial motility, flagellar rotation

Introduction

When grown on a moist nutrient-rich medium, many flagellated bacteria elongate, produce wetting agents, and colonize the surface by swimming outward in densely-packed groups within a thin layer of fluid, a process known as swarming (1-3). Swarming promotes invasiveness and virulence of infectious pathogens (2). It is regulated by pathways that enable cells to choose between swimming or forming sessile biofilms (4). A model system that we study is the bacterium *Escherichia coli*, which was shown to swarm by Harshey & Matsuyama (5). Our focus is on swarm mechanics, how cells move and how this motion is promoted by flagellar rotation (6-8); see also (9-11).

However, little is known about the swarm fluid, despite its significance to the expansion and physiology of swarms. The swarm fluid is important for swarm expansion, not only because it supports the operation of flagella (12), but also because it carries nutrients that support growth or molecules that regulate cellular functions, such as signals involved in quorum-sensing (13-14). Quorum-sensing has been found to regulate the synthesis of biosurfactants that facilitate swarming in *Bacillus subtilis* (15-16), *Serratia liquefaciens* (17) and *Pseudomonas aeruginosa* (18). The quorum-sensing molecules involved in these systems are released from cells and diffuse in the swarm fluid before entering cells again.

The layer of swarm fluid can be as thin as the width of a cell (~1 μm) and even thinner near the swarm edge (8). This makes it difficult to probe the hydrodynamics of swarm fluid with conventional micro-fluid markers, such as polystyrene microspheres (19). Large markers tend to be entrained by cells within the body of the swarm, while small ones become embedded in the agar. We solved this problem by developing buoyant fluid markers: microbubbles that

form spontaneously when a suspension of droplets of a water-insoluble surfactant is exposed to an air-liquid interface. With these novel markers, we discovered an extended stream (or river) flowing clockwise along the leading edge of *E. coli* swarms. Flow rates of order 10 μm/s (~3 times the rate of swarm spreading) persist over long distances, providing the swarm with an avenue for long-range communication. The findings shed new light on how swarming bacteria might regulate material transport, broaden our understanding of flagellar hydrodynamics (20), and have implications for the engineering of bacterial-driven microfluidic devices (21-22).

Results

Microbubble formation

When a drop of a suspension of Span 83 (a water-insoluble surfactant with nonionic head groups derived from sorbitol and hydrophobic tails derived from common fatty acids, primarily oleic acid; see Methods) is placed on an agar surface a few cm in front of an *E. coli* swarm, the water is absorbed by the agar and the Span 83 droplets are exposed to air. The droplets explode into large films, which soon contract and transform into arrays of micron-sized objects by a cascade of sudden events, as shown in Fig. 1, or into a single micron-sized object that can be much larger than the original droplet, as shown in Fig. S1. These objects appear to be air bubbles, air-filled capsules with surfactant walls. The initial explosion of surfactant droplets usually is complete within 1/15 s (2 video frames), while the contraction and bubble formation takes variable amounts of time. The films that form appear to be similar to the macroscopic ones studied by Matar & Troian (23), but the subsequent contraction and bubble formation appears to be new and merits further study. The explosions are reminiscent of those described recently for large interfacial air bubbles by Bird et al. (24) and

might share a similar mechanism. In any event, the microbubbles formed in this way move continuously among cells within the swarm, indicating that they can easily follow fluid flow. In contrast, untransformed surfactant droplets of a similar size show only intermittent movement within swarms or get stuck in the agar.

Long-range clockwise flow along *E. coli* swarm edges

As the swarm approaches, the bubbles move quite smoothly along the swarm edge; although, the bodies of cells near the swarm edge show limited or even no movement. Surprisingly, the direction of net movement of the bubbles is always clockwise (CW) when the swarm is viewed from above (found with >30 swarms). An example is shown in Figs. 2*A*, *B*. This movement can persist over long distances. We observed one microbubble moving CW along the swarm edge at an average speed of ~8 μm/s for a distance of over 0.5 mm. These observations suggest the existence of long-range unidirectional flow, i.e., a river, along the edge of *E. coli* swarms. Such a river might establish right-handed chirality in swarms if a colony branches, because cells tend to move onto virgin agar where there is sufficient liquid for them to spin their flagella. Indeed, we observe such right-handedness in young swarms of *E. coli*, as shown in Fig. 2*C*.

Submicron bubbles (<1.0 μm in diameter) continuously varied their speed and distance from the swarm edge (defined as the distance from the bubble to the nearest cell body) and provided a tool for probing the flow-rate profile of the river. From the trajectory for each bubble, we measured the velocity and the distance to the swarm edge in every video frame (30 times per s). The velocity was divided into tangential and radial components (along the swarm edge and in the direction of swarm expansion, respectively). The average tangential and radial velocities at a specific distance from the swarm edge were taken as the average tangential and radial flow rates of the river at that distance from the swarm edge.

We collected such data for each of three *E. coli* swarms (strain HCB1668). The average tangential and radial flow-rate profiles for one of these swarms are plotted in Figs. 3*A*, *B*. The tangential flow profile peaks at a distance of 2-2.5 μm, about half of the average length of the flagellar filaments (7), at a flow rate of ~8 μm/s. The other two swarms showed similar tangential flow profiles. The tangential flow rate drops to nearly zero at the distance of ~7 μm, suggesting that the average width of the river is ~7 μm. Because cells at the swarm edge tend to project their flagella outwards onto the virgin agar when they get stuck (7, 9), the river flow is most likely generated by the rotating flagella of these stuck cells, which form a special kind of bacterial carpet (25). The radial flow rate within the distance of one flagellar length is close to the expansion rate of the swarm (3.3 μm/s). This supports the notion that swarm expansion is aided by flagella pumping fluid outwards from the edge of the colony (6-7, 9).

Local chiral flow patterns

We found other asymmetric flow patterns on the scale of single cells. When the edge of a dense *E. coli* swarm (with microbubbles already formed) is diluted by a small amount of external liquid (such as growth medium), microbubbles move in exclusively counterclockwise (CCW) swirls in between the immobile cells (>50 samples). Fig. S3 shows such an example, in which a bubble makes 12 CCW circles in 13.35 s (0.9 revolutions per s). The rotational frequency of the swirling motion varies from cell to cell and from time to time, most likely depending upon the amount of surrounding fluid.

To better understand the CW river and the CCW swirls just described, we wanted to probe the flow generated by single cells near the swarm edge. However, the swarm edge is densely packed with cells, and it is impossible to discern the flow

generated by individual cells. Instead, we collected cells at the swarm edge in motility buffer and dropped this cell suspension on a coverslip coated with a thin layer of agar (see Methods), creating a sparse distribution of isolated cells and a denser array of cells near the drying edge of the drop. Like cells near the swarm edge, the cells near the drying edge of the drop have limited movement most likely due to the lack of surrounding liquid, but they also create long-range CW flows along the edge of the cell array and CCW swirls in between cells (see Video S5). Therefore, this system (referred to as the "agar slip model") allows one to observe isolated cells under conditions that mimic those observed near a real swarm edge.

By tracking the motion of microbubbles around isolated cells in the agar slip model, we found that bubbles circle around cell bodies exclusively CW (>50 samples, one of which is shown in Fig. S4). This suggests CW flow circulations around cells residing in a thin liquid layer on a solid surface. CCW swirls in between several immobile cells can be explained as the net effect of CW circulations around each individual cell. Similarly, the long-range CW flow along a swarm edge can be explained as the net effect of CW flows around cells that are lined up along the swarm edge.

All of the flow patterns observed with *E. coli* were seen as well with strains of *B. subtilis* (DS3610) (26) and *S. marcescens* (ATCC274) (27) grown on Eiken agar (see Methods). These observations suggest that such flows generally occur with peritrichously-flagellated bacteria near solid surfaces.

Asymmetric flows correlate with CCW-biased flagellar rotation

To find out the origin of CW circulation around individual cells, we imaged microbubbles and cell bodies in phase-contrast and flagellar filaments in fluorescence (see Methods). In the agar slip model, as a swarm cell approaches shallow fluid near the edge of the drop and becomes stuck, the flagella unbundle, and the filaments project outwards and roll CW, as shown in Fig. 4. Although the flagella fail to propel cells under these circumstances, they continue to rotate and frequently change their directions of rotation. The sense of this rotation could be inferred from the direction of the roll and the shape of the filaments. The flagella appear to have a CCW rotational bias similar to that found with swimming cells, because they prefer to roll CW (conspicuous in 10 of the 15 examples), as expected for normal (left-handed) helices spinning CCW close to a solid surface (28). This observation suggests two ways in which CW flow around the cells might be generated: when a CCW-rotating filament approaches the surface, it is swept CW, which moves fluid CW; once a filament is oriented in this way, it will pump fluid CW, since a left-handed helical filament spinning CCW moves fluid away from its base in a direction parallel to the helical axis. A mechanism of this kind has been proposed for the generation of flows around stuck cells of *B. subtilis* (29). Cells in a swarm swim without curving strongly to the right or the left (6), suggesting that they move between two fixed surfaces, apparently a stationary surfactant layer above and an agar surface below. This proposition was proved by the relative immobility of small particles of MgO smoke deposited on the upper surface of the swarm (8). However, cells near the edge of a swarm or in the agar slip model are stuck to the agar and not swimming freely, so it is likely that their flagellar filaments are closer to the agar, on average, than to the air/water interface, and thus are oriented CW. No flows were observed with cells lacking flagellar filaments (HCB1688 grown without a *fliC* inducer) or with cells having paralyzed flagella (HCB84), so rotating filaments are absolutely required.

Discussion

We found a novel method for making microbubbles that serve as tracers for fluid flow in bacterial swarms, and with these tracers discovered an array of interesting chiral flow patterns: a river flowing CW in front of the swarm, CW swirls around isolated cells, and CCW swirls in between cells in sparse arrays. The origin of these flow patterns is due to CCW-biased flagellar rotation, when left-handed helical filaments projecting out from cells and spinning CCW roll CW over the underlying surface and pump fluid CW.

As noted earlier, the layer of fluid in a swarm provides not only an environment that enables cells to spin their flagella, but also a vehicle for the transport of nutrients or molecules secreted by cells, e.g., those involved in quorum sensing. Long-distance transport is generally more effective when it occurs by bulk flow than by diffusion alone. With bulk flow, displacement is proportional to time; with diffusion, displacement is proportional to the square root of the time. So, given enough time, bulk flow always wins (30). A small molecule carried by a stream flowing at 8 μm/s at the swarm edge will outdistance one diffusing in the same direction in a static medium after about 30 s. However, such transport will not work for a stream flowing over agar, because the small molecule will diffuse out of the stream into the underlying agar. Thus, we find it very interesting that some of the signaling molecules involved in quorum sensing are packaged in membrane vesicles (31) and that membrane vesicles are commonly seen in biofilms (32). Cells of *P. aeruginosa* produce hydrophobic quinolone signals (PQS) involved in the regulation of the synthesis of biosurfactants that facilitate swarming (33). PQS have been shown to be packaged in secretory membrane vesicles, which then traffic the signals between cells to coordinate group behavior (31).

Membrane vesicles of this size (diameter of order 100 nm) are produced by many bacterial species, including *E. coli* (32). Since vesicle diffusion coefficients are quite small, flow of swarm fluid will greatly enhance their transport, providing an avenue for long-range communication in the swarming colony. If a swarm is facing environmental stress, long-range communication could enable unaffected regions of the colony to turn on specific responses in ample time. Cells in swarms are known to have higher resistance to a variety of antimicrobial agents than cells in liquid cultures (34-36). We wonder whether colonization by swarming of pathogenic bacteria might be blocked by modification of surface properties required for the generation of fluid flows, instead of through perturbation of swarm-cell biochemistry.

Materials and methods

Bacterial strains. The *E. coli* strains used for this study were AW405 (wild type), HCB84 (*motA448*) (37) and HCB1668 (FliC S353C), an AW405 derivative whose flagellar filaments can be labeled with thiol-reactive fluorescent dyes (7). *B. subtilus* (DS3610) (26) and *S. marcescens* (ATCC274) (27) also were used. Single-colony isolates were grown overnight in LB medium (1% Bacto tryptone, 0.5% yeast extract, and 0.5% NaCl, pH 7.5) at 30ºC to stationary phase. For *E. coli* HCB1668, kanamycin (50 μg/ml), chloramphenicol (34 μg/ml), and arabinose (0.5%) were added to the growth medium. These cultures were diluted 10^{-5} to provide cells for inoculation of swarm plates.

Swarm plates. For *E. coli*, the swarm agar was 0.45% (AW405) or 0.6% (HCB1668) Eiken agar in 1% Bacto peptone, 0.3% beef extract, and 0.5% NaCl. For *B. subtilus* and *S. marcescens*, Eiken agar was respectively 0.8% and 0.6% in

the medium just described. When grown on 0.8% Eiken agar, *B. subtilus* swarms exhibited a cell density at the swarm edge comparable to that of *E. coli* grown on 0.45% Eiken agar. The swarm agar was autoclaved and stored at room temperature. Before use, the agar was melted in a microwave oven, cooled to ~60ºC, and pipetted in 25 mL aliquots into 150 x 15 mm polystyrene petri plates. For *E. coli* HCB1668, antibiotics and arabinose were added to the liquefied swarm agar before pipetting at the concentrations used in liquid cultures. The plates were swirled gently to ensure complete wetting, and then cooled for 30 min without a lid inside a large Plexiglas box. Drops of diluted cell culture (2 μL, described above) were inoculated at a distance of 2-3 cm from the edges of the plates, and the plates were dried for another 30 min without a lid, covered, and incubated overnight at 30ºC and 100% relative humidity until the swarms grew to sufficient size.

Preparation of surfactant suspensions. A drop of the water-insoluble surfactant Span 83 (Sorbitan sesquioleate, S3386, Sigma-Aldrich) was mixed with de-ionized water in a glass bottle at a wt/wt ratio of 0.03-0.04%. Air was injected at the bottom of the mixture through a narrow plastic tube, resulting in an uprising of bubbles that accelerated the breakdown of Span 83 droplets. This was done for >1 h, until the surfactant suspension became milky. When viewed with a phase-contrast microscope, the suspension appeared full of refractile Span 83 droplets with diameters ranging from a fraction of a μm to a few μm.

Preparation of agar coverslip samples (agar slip model). Swarm cells were collected by gently rinsing the leading edge of the swarm with motility medium (0.01 M potassium phosphate pH 7.0, 0.067 M NaCl, 10^{-4} M EDTA), as described previously (7), except that Tween 20 was not used. When we needed to

visualize flagellar dynamics, cells of *E. coli* HCB1668 were fluorescently labeled at this point with Alexa Fluor 532 C_5 maleimide (Invitrogen-Molecular Probes), as described previously (7), except that Tween 20 was not used. We placed 1 μl of Span 83 suspension on top of a 20 x 20 mm patch of thin agar (0.6%) that had been freshly poured on a 24 x 60 mm No. 1 coverslip (#48393-106, VWR, West Chester, PA), pre-cleaned with saturated solution of KOH in ethanol. We put the sample in a 100% relative-humidity chamber and waited 0.5 to 1 h until the drop was absorbed by the agar and the microbubbles formed. Then 2 μl of cell suspension was added where the Span 83 had been added, and the sample was immediately covered with a 1x3-inch microscope slide (#48300-047, VWR) placed on 1-mm thick (10 x 24-mm) shims cut from a similar slide. Then this preparation was transferred from the humidity chamber to the microscope stage for imaging. Cells could be imaged for at least 10 min without noticeable evaporation.

Phase contrast and epifluorescence imaging. The motion of microbubbles and filaments around cell bodies stuck to the agar substrate were observed simultaneously in phase contrast and epifluorescence, respectively, with a 40x phase-contrast objective mounted on a Nikon Diaphot 200 inverted microscope. Phase-contrast illumination was provided by a yellow LED, and fluorescence excitation was provided by an argon-ion laser, as described below, switched on and off in synchrony with alternate lines of a 2:1-interlaced video recording. Recordings were made with a CCTV camera (model KPC-650BH, KT&C, Korea) and a digital tape recorder (model GV-D1000, Sony). The video sequences were transferred to a PC as “avi” files and uncompressed using the free software VirtualDub (http://www.virtualdub.org/). Separate phase-contrast and fluorescence sequences were assembled by deinterlacing with custom software written in Matlab (The MathWorks, Inc., Natick, MA) and replacing the missing

lines with pixels that were the arithmetic means of the pixels above and the pixels below. Two synchronized multi-page tiff images were generated for further analysis.

The phase-contrast light source was a yellow LED (# OVLGY0C9B9, TT Electronics/Optek Technology, Carrollton, Texas) powered by custom-built electronics and placed about 75 mm above the phase ring of the microscope condenser. The epifluorescence light source was an argon-ion laser (Stabilite 2017, Spectra-Physics, Santa Clara, CA) tuned to 514 nm. The laser exposure time was controlled with an an electro-optical deflector (EOD, model # 310A, Conoptics, Danbury, CT), which deflected the laser beam through the aperture of a pinhole (“on”) or away from this aperture (“off”). The EOD was driven by two power supplies (HP 6515A, Palo Alto, CA) set to 750 V via a custom-built three-state switch (designed by Winfield Hill, model # RIS-688, Rowland Institute at Harvard, Cambridge, MA): +1500 V for "on", -1500 V for “off”, and 0 V in between experiments to protect the EOD crystal.

The microscope was modified for laser illumination by rotating the fluorescence cube in a custom-designed mount 90° around the vertical axis to allow excitation from the right side. We used a dichroic mirror (527DCLP, Chroma Technology Corp., Bellows Falls, VT) without excitation or emission filters; however, the excitation light was blocked in the emission channel with a thin-film, single-notch filter (NF01-514U-25, Semrock, Rochester, NY). Custom-built electronics controlled the timing and the exposure times (i.e., the length of the “on” states of the two light sources), in synchrony with the video vertical sync pulse. The exposure time for both phase and laser illumination varied between 40 and 320 μs.

Data analysis. Microbubbles were tracked in the phase-contrast video sequences manually using the MTrackJ plugin (Erik Meijering, http://www.imagescience.org/meijering/software/mtrackj/) developed for ImageJ (http://rsbweb.nih.gov/ij/). The track data were then analyzed to yield the bubble speed and the distance from bubble to swarm edge. We inferred the size of microbubbles by doing Gaussian fits to the light-intensity profile of a line crossing the bubble center plotted in ImageJ. The widths of Gaussian fits (2σ) were taken as the diameter of bubbles. As a validation to this method, it yields values for cell widths consistent with other experimental data, about 0.8 μm.

Acknowlegments. We thank Peko Hosoi, Daniel Kearns and Richard Losick for comments on the manuscript, and Linda Turner, Rongjing Zhang and Junhua Yuan for discussions and help with the experiments. This work was supported by grants AI065540 and AI016478 from the National Institutes of Health.

References

1. Copeland MF & Weibel DB (2009) Bacterial swarming: a model system for studying dynamic self-assembly. *Soft Matter* 5:1174-1187.
2. Harshey RM (2003) Bacterial motility on a surface: many ways to a common goal. *Annu. Rev. Microbiol.* 57:249-273.
3. Kearns DB (2010) A field guide to bacterial swarming motility. *Nat. Rev. Microbiol.* 8:634-644.
4. Verstraeten N*, et al.* (2008) Living on a surface: swarming and biofilm formation. *Trends Microbiol.* 16:496-506.

5. Harshey RM & Matsuyama T (1994) Dimorphic transition in Escherichia coli and Salmonella typhimurium: surface-induced differentiation into hyperflagellate swarmer cells. *Proc Natl Acad Sci U S A* 91(18):8631-8635.
6. Darnton NC, Turner L, Rojevsky S, & Berg HC (2010) Dynamics of bacterial swarming. *Biophys. J.* 98:2082-2090.
7. Turner L, Zhang R, Darnton NC, & Berg HC (2010) Visualization of flagella during bacterial swarming. *J. Bacteriol.* 192:3259-3267.
8. Zhang R, Turner L, & Berg HC (2010) The upper surface of an *Escherichia coli* swarm is stationary. *Proc. Natl. Acad. Sci. USA* 107:288-290.
9. Copeland MF, Flickinger ST, Tuson HH, & Weibel DB (2010) Studying the dynamics of flagella in multicellular communities of *Escherichia coli* using biarsenical dyes. *Appl. Environ. Microbiol.* 76:1241-1250.
10. Zhang HP, Be'er A, Smith RS, Florin E-L, & Swinney HL (2009) Swarming dynamics in bacterial colonies. *EPL* 87:48011.
11. Zhang HP, Be'er A, Florin E-L, & Swinney HL (2010) Collective motion and density fluctuations in bacterial colonies. *Proc. Natl. Acad. Sci. USA* 107:13626-13630.
12. Dechesne A, Wang G, Gülez G, Or D, & Smets BF (2010) Hydration-controlled bacterial motility and dispersal on surfaces. *Proc. Natl. Acad. Sci. USA* 107:14369-14372.
13. Fuqua C, Winans SC, & Greenberg EP (1996) Census and consensus in bacterial ecosystems: the LuxR-LuxI family of quorum-sensing transcriptional regulators. *Annu Rev Microbiol* 50:727-751.
14. Daniels R, Vanderleyden J, & Michiels J (2004) Quorum sensing and swarming migration in bacteria. *FEMS Microbiol. Rev.* 28:261-289.

15. Magnuson R, Solomon J, & Grossman AD (1994) Biochemical and genetic characterization of a competence pheromone from *B. subtilis*. *Cell* 77:207–216.
16. Kearns DB & Losick R (2003) Swarming motility in undomesticated *Bacillus subtilis*. *Mol Microbiol* 49:581-590.
17. Lindum PW*, et al.* (1998) N-acyl-L-homoserine lactone autoinducers control production of an extracellular surface-active lipopeptide required for swarming motility of *Serratia liquefaciens* MG1. *J Bacteriol* 180:6384-6388.
18. Kohler T, Curty LK, Barja F, Van Delden C, & Pechere JC (2000) Swarming of *Pseudomonas aeruginosa* is dependent on cell-to-cell signaling and requires flagella and pili. *J Bacteriol* 182: 5990–5996.
19. Wu X-L & Libchaber A (2000) Particle diffusion in a quasi-two-dimensional bacterial bath. *Phys. Rev. Lett.* 84:3017-3020.
20. Lauga E & Powers TR (2009) The hydrodynamics of swimming microorganisms. *Rep. Prog. Phys.* 72:096601.
21. Kaehr B & Shear JB (2009) High-throughput design of micrtofluidics based on directed bacterial motility. *Lab Chip* 9:2632-2637.
22. Kim MJ & Breuer KS (2008) Microfluidic pump powered by self-organizing bacteria. *Small* 4:111-118.
23. Matar OK, Troian, S. M. (1997) Linear stability analysis of an insoluble surfactant monolayer spreading on a thin liquid film. *Phys Fluids 9, 3645* 9(12):3645-3657.
24. Bird J, de Ruiter R, Courbin L, & Stone HA (2010) Daughter bubble cascades produced by folding of ruptured thin films. *Nature* 465:759-762.
25. Darnton N, Turner, L., Breuer, K., Berg, H.C. (2004) Moving fluid with bacterial carpets. *Biophys J* 86(3):1863-1870.

26. Blair KM, Turner, L., Winkelman, J. T., Berg, H. C., Kearns, D. B. (2008) A molecular clutch disables flagella in the Bacillus subtilis biofilm. *Science* 320(5883):1636-1638.
27. Alberti L, Harshey, R. M. (1990) Differentiation of Serratia marcescens 274 into swimmer and swarmer cells. *J Bacteriol* 172(8):4322-4328.
28. Lauga E, DiLuzio WR, Whitesides GM, & Stone HA (2006) Swimming in circles: motion of bacteria near solid boundaries. *Biophys. J.* 90:400-412.
29. Cisneros LH, Kessler JO, Ortiz R, Cortez R, & Bees MA (2008) Unexpected bipolar flagellar arrangements and long-range flows driven by bacteria near solid boundaries. *Phys. Rev. Lett.* 101:168102.
30. Berg HC (Random Walks in Biology. *(Princeton Univ. Press, Princeton, 1993)*.
31. Mashburn LM, Whiteley, M. (2005) Membrane vesicles traffic signals and facilitate group activities in a prokaryote. *Nature* 437(7057):422-425.
32. Schooling SR, Beveridge, T. J. (2006) Membrane vesicles: an overlooked component of the matrices of biofilms. *J Bacteriol* 188(16):5945-5957.
33. McKnight SL, Iglewski BH, & Pesci EC (2000) The Pseudomonas quinolone signal regulates rhl quorum sensing in *Pseudomonas aeruginosa*. *J Bacteriol* 182:2702-2708.
34. Kim W, Killam T, Sood V, & Surette MG (2003) Swarm-cell differentiation in *Salmonella enterica* serovar typhimurium results in elevated resistance to multiple antibiotics. *J. Bacteriol.* 185:3111-3117.
35. Lai S, Tremblay J, & Déziel E (2009) Swarming motility: a multicellular behaviour conferring antimicrobial resistance. *Env. Microbiol.* 11:126-136.
36. Butler MT, Wang Q, & Harshey RM (2010) Cell density and mobility protect swarming bacteria against antibiotics. *Proc. Natl. Acad. Sci. USA* 107:3776-3781.

37. Yuan J & Berg HC (2008) Resurrection of the flagellar rotary motor near zero load. *Proc Natl Acad Sci U S A* 105:1182-1185.

Figure Legends

Fig. 1. Bubble formation cascade. The highly refractive surfactant droplet seen by bright-phase microscopy at the center of *A* first explodes into a less bright or even invisible film that spreads over a much larger area than the size of the droplet (*B*-*C*). The film then contracts and bubbles form at the periphery of the film (*D*-*E*). The film contraction proceeds and a second round of bubble formation takes place (*E*-*F*), resulting in many bright air bubbles all over the area previously occupied by the film. The bubbles shown here have a minimum diameter of ~1.0 μm and a maximum diameter of ~2.0 μm. They remain stable for up to 5 h on agar under our experimental conditions (see Methods). Scale bar at the lower right-hand corner of *F* is 10 μm long. See Video S1.

Fig. 2. Asymmetric flow and colony patterns. A 0.2 μL drop of a suspension of Span 83 was placed at a distance of 3-5 cm ahead of an *E. coli* swarm (HCB1668). Microbubble formation was complete within ~10 min but the swarm took 3-5 h to reach the bubbles. By this time the water in the Span 83 suspension had been absorbed by the agar and thus had little effect on the swarm. (*A*-*B*) The two panels show a small section of the advancing swarm edge, with the swarm moving from left to right. One microbubble (2.2 μm in diameter, indicated by the white arrows) moves downward along the swarm edge, or CW when the swarm is viewed from above. The bubble traveled a distance of 87.4 μm over 6.23 s at an average speed of 14.0 μm/s. For comparison, the swarm expansion rate was 3.2 μm/s. Scale bar at the lower right-hand corner of *B* is 10 μm long. See Video S3. (*C*) The right-handed colony pattern of a young swarm of *E. coli* AW405. Most branches of the swarm curve clockwise. Scale bar at the lower right-hand corner of *C* is 0.5 cm long.

Fig. 3. Flow profile of the river for one swarm. (*A*) Average tangential flow rate versus the distance from the swarm edge, computed from 28 bubble trajectories. The dashed line is a Giddings peak function fit using the software Origin 6.1 (OriginLab Corp., Northampton, MA). Two other swarms showed similar tangential flow profiles (see Fig. S2). (*B*) Average radial flow rate versus the distance form the swarm edge. Error bars are standard deviations for the ensemble of bubble trajectories.

Fig. 4. Correlation between CW bubble circulation and CW rolling of flagellar filaments. In *A*-*E* the flagellar filaments (bright hairy structures) move clockwise around the cell body (the rod-shaped object at the center of each panel), which is stuck to the agar slip. This movement is most evident when following the bundle of filaments indicated by the white arrow. Meanwhile, a microbubble (the gray spot) circulates CW around the cell. The phase-contrast image of the cell body was cropped from the image taken for the first panel, and its contrast was enhanced and smoothed in ImageJ (http://rsbweb.nih.gov/ij/); the enhanced image was superimposed on the fluorescence images shown in *A*-*E*. Phase-contrast images of the microbubble were plotted directly onto the corresponding fluorescence images and highlighted as gray spots. *F* is the processed phase-contrast image of the cell and microbubble (highlighted as a white spot) at the time of 0.4 s, with the bubble trajectory from *A* to *E* plotted as a black curve. Scale bar at the lower right-hand corner of *F* is 5 μm long. See Videos S7 and S8.

Figures

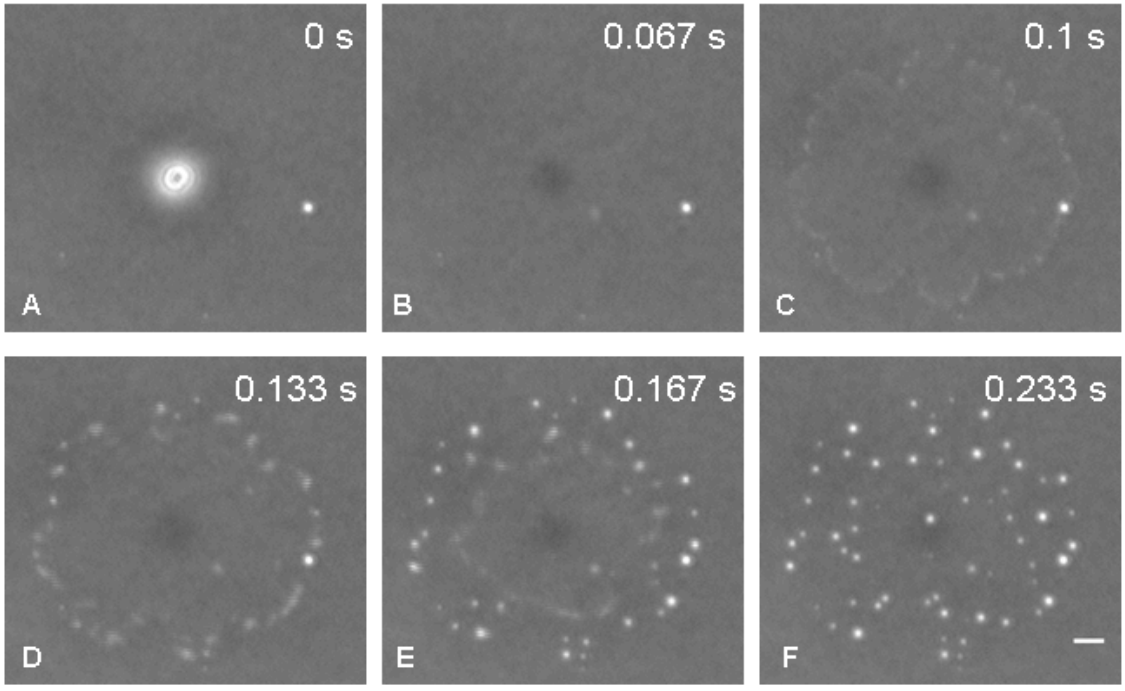

Fig. 1

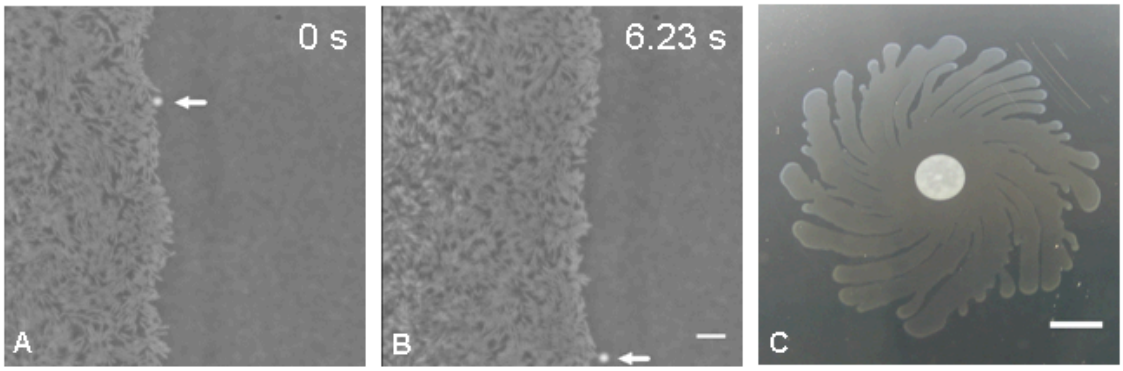

Fig. 2

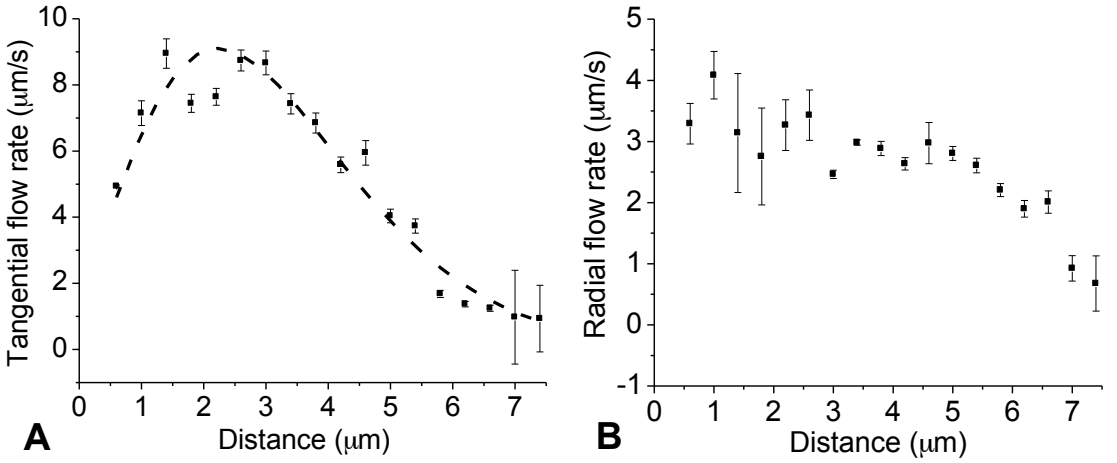
Tangential flow rate (μm/s)
Distance (μm)
A
Radial flow rate (μm/s)
Distance (μm)
B

Fig. 3

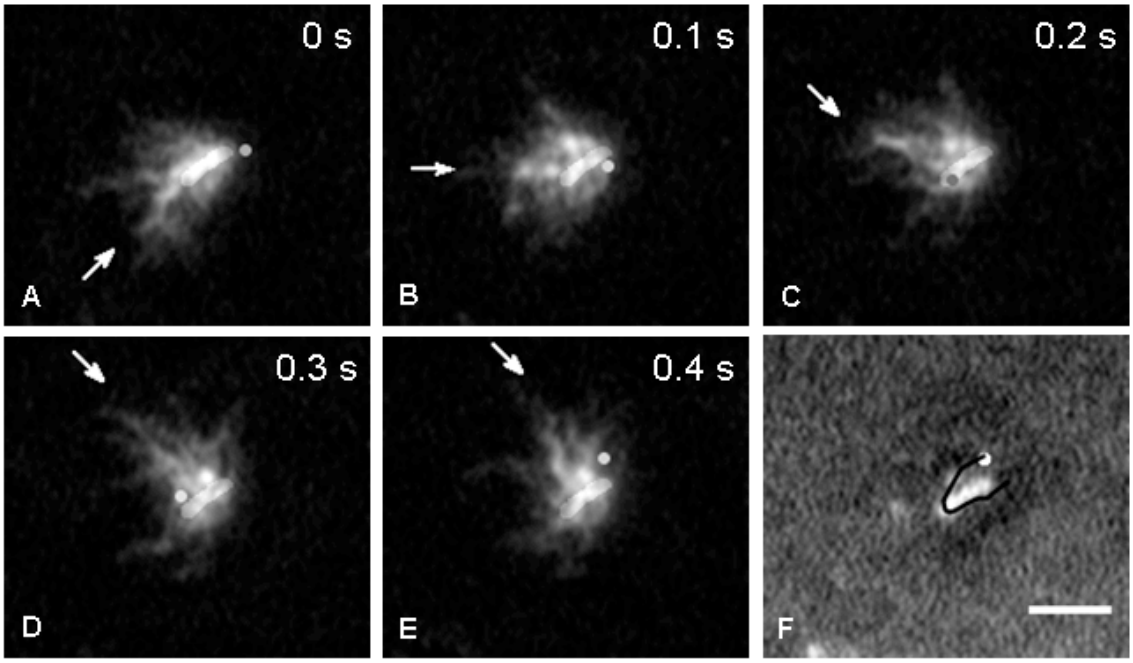
0 s
A
0.1 s
B
0.2 s
C
0.3 s
D
0.4 s
E
F

Fig. 4

Supporting Information

Supporting Figures

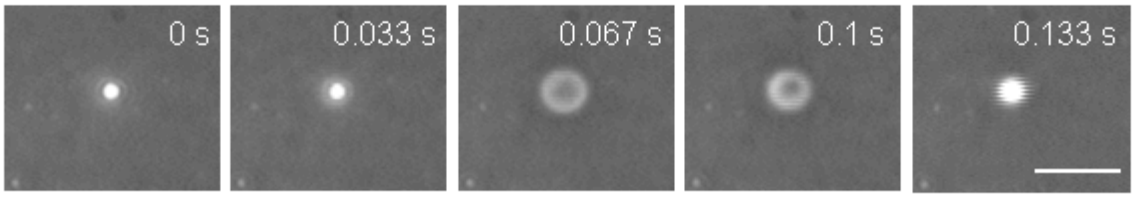

Fig. S1. Single bubble formation. The surfactant droplet in *A* first explodes into a rounded object that is much larger but less bright, as shown in panel *C*, which is probably a transient air bubble similar to the ones found at the periphery of the film shown in Fig. 1*D* of the main text. Following the explosion, this object in panel *C* contracts into a single bubble, which is highly refractive (*C*-*E*). The diameter of the bubble shown in panel *E* is twice that of the original droplet shown in panel *A*. Scale bar at the lower right-hand corner of panel *E* is 10 μm long. See Video S2.

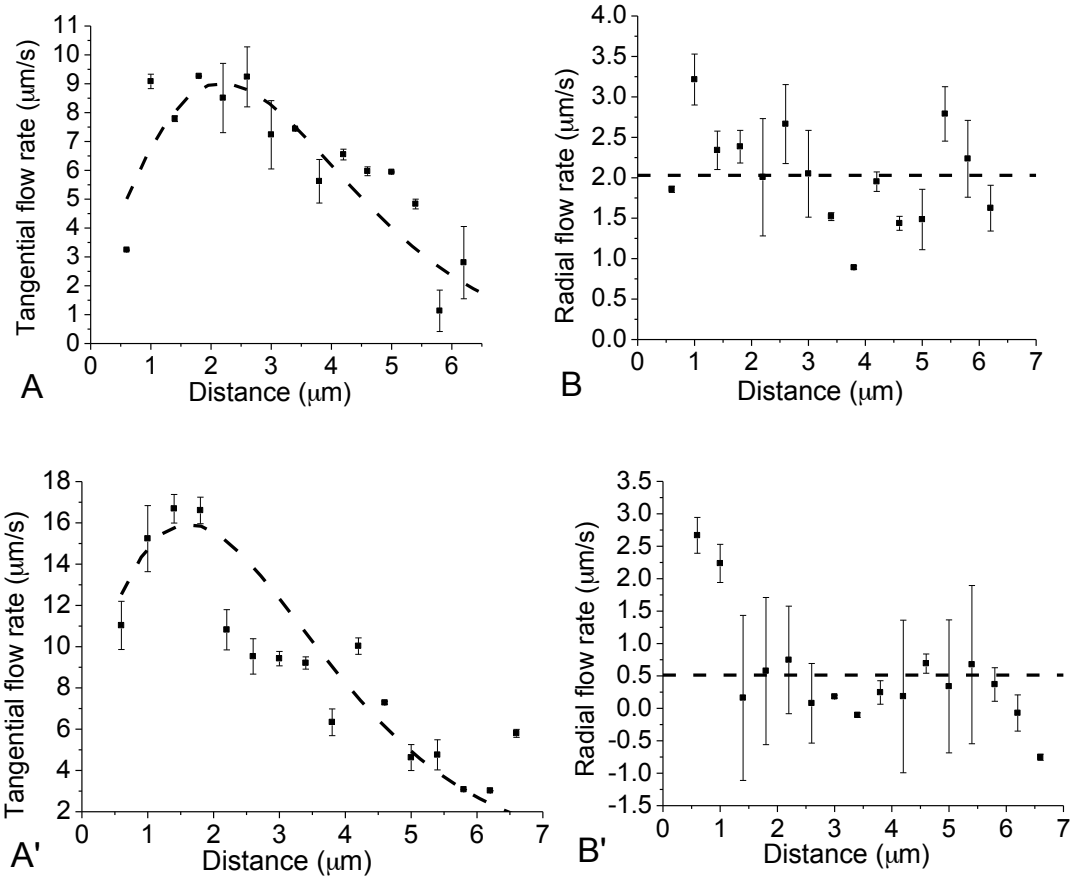

Fig. S2. **Flow profile of the river for two other swarms (*E. coli* HCB1668)**. (*A*) Average tangential flow rate versus the distance from the swarm edge, computed from 24 bubble trajectories. The dashed line is a Giddings peak function fit using the software Origin 6.1 (OriginLab Corp., Northampton, MA). (*B*) Average radial flow rate versus the distance form the swarm edge computed from 28 bubble trajectories. Error bars are standard deviations for the ensemble of trajectories. The swarm for panels *A* and *B* expanded at a rate of 1.7 μm/s. The swarm for panels *A*' and *B*' expanded at a rate of 0.8 μm/s. The tangential flow profile of the river at the swarm edge is similar in the three swarms (including the one described in the main text): all have a peak flow rate at a distance of ~2 μm and extend to a distance of ~7 μm. The radial flow profile varies with the swarm expansion rate, as expected, and the mean flow rate (indicated by the

dashed lines in panels *B* and *B*') is close to the swarm expansion rate.

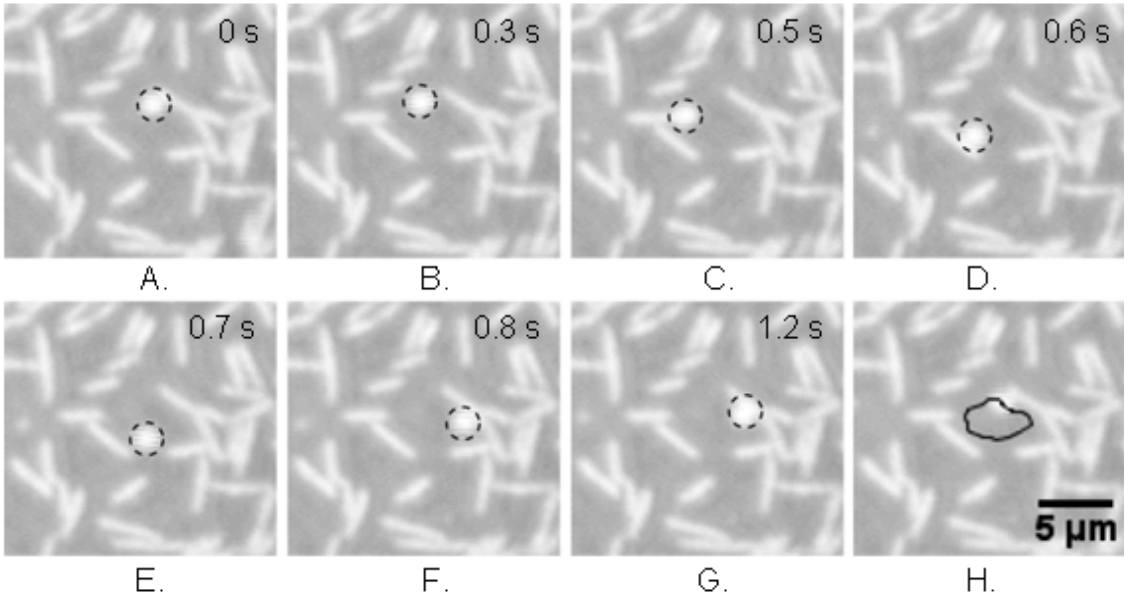

Fig. S3. **CCW swirl in between cells.** The image sequence (panels *A*-*G*) shows a full circle of CCW motion of a microbubble (~1.2 μm in diameter, circled by a dashed black line) in between immobile cells (white rod-shaped objects) obtained by dilution at an *E. coli* swarm edge (strain HCB1668). The bubble makes 12 such circles in 13.35 s (0.9 revolutions per s). The rotational frequency of the swirling motion varies from case to case and from time to time, most likely depending upon the amount of surrounding fluid. Panel *H* shows the bubble trajectory (black curve) from panels *A*-*G* plotted in the background of panel *G*. See Video S4.

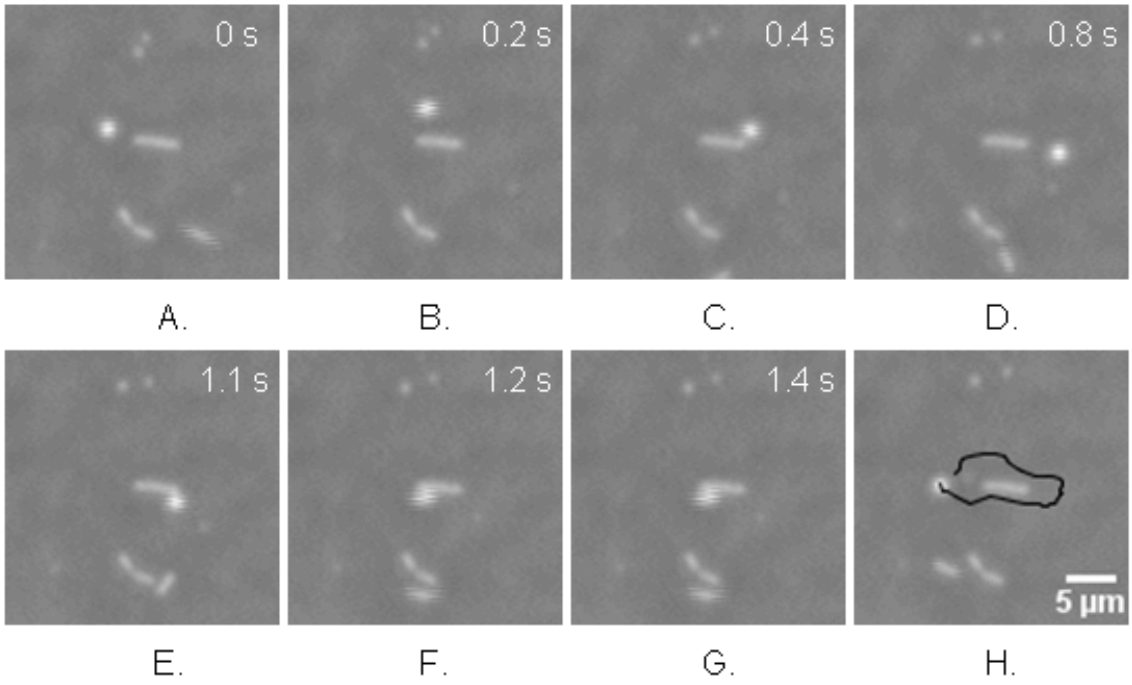

Fig. S4. **CW movement of a microbubble around an isolated cell.** The image sequence (panels *A*-*G*) shows a microbubble (~1.2 μm in diameter) making a nearly full CW circle in 1.4 s around the cell (*E. coli* HCB1668) in the center of each panel. Panel H shows the bubble trajectory (black curve) from panels *A*-*G* plotted in the background of panel *G*. As in Fig. S3, the circling frequency varies, most likely depending upon the amount of liquid surrounding the cell. See Video S6.

Legends of Supporting Videos

Video S1. Bubble formation cascade. The display speed is slowed down by a factor of 30, to 1 frame per second.

Video S2. Single bubble formation. The display speed is slowed down by a factor of 30, to 1 frame per second.

Video S3. Clockwise river flow at swarm edge. This real-time movie shows a microbubble (2.2 μm in diameter) being transported by the river along a swarm edge (*E. coli* HCB1668) in a clockwise direction (when the swarm is viewed from above). The bubble travels a distance of 87.4 μm in 6.23 s at an average speed of 14.0 μm/s. The speed of the bubble movement and the distance from the bubble to the swarm edge vary continuously. Readers are invited to watch more movies of *E. coli* swarms on our website (http://www.rowland.harvard.edu/labs/bacteria/movies_swarmecoli.html).

Video S4. CCW swirl in between cells (*E. coli* HCB1668). This real-time movie shows a microbubble making 12 full circles CCW in 13.35 s, ~0.9 revolutions per second.

Video S5. The agar slip model. This real-time movie shows the motion of cells (*E. coli* HCB1668) and microbubbles on an agar slip right after the drop of cell suspension was added. The preparation creates a sparse distribution of isolated cells, which are now swimming actively but will soon get stuck as the water in the drop is absorbed by the agar. A denser array of cells will appear near the drying edge of the drop. Like cells near the swarm edge, the cells near the drying edge of the drop have limited movement due to the lack of surrounding liquid. However,

they also create extensive CW flows along the edge of the cell array and CCW swirls in between cells, which are evident from the movement of microbubbles.

Video S6. CW movement of a microbubble around an isolated cell (*E. coli* HCB1668). This real-time movie shows a microbubble (~1.2 μm in diameter) making a nearly full CW circle around the cell in 1.4 s.

Video S7. Unprocessed real-time phase-contrast video of the cell (*E. coli* HCB1668) and the microbubble shown in Fig. 4 of the main text.

Video S8. Unprocessed real-time fluorescence video of the flagellar motion shown in Fig. 4 of the main text.